Talanta 108 (2013) 11–18

Contents lists available at SciVerse ScienceDirect

Talanta

journal homepage: www.elsevier.com/locate/talanta

Label-free detection of glycoproteins by the lectin biosensor down to attomolar level using gold nanoparticles

Tomas Bertok [a], Alena Sediva [a], Jaroslav Katrlik [a], Pavol Gemeiner [b], Milan Mikula [b], Martin Nosko [c], Jan Tkac [a,*]

[a] Department of Glycobiotechnology, Institute of Chemistry, Slovak Academy of Sciences, Dúbravská cesta 9, 845 38 Bratislava, Slovak Republic
[b] Department of Graphic Arts Technology and Applied Photochemistry, Faculty of Chemical and Food Technology, Slovak University of Technology, Radlinského 9, 812 37 Bratislava, Slovak Republic
[c] Institute of Materials and Machine Mechanics, Slovak Academy of Sciences, Račianska 75, 831 02 Bratislava, Slovak Republic

ARTICLE INFO

Article history:
Received 11 October 2012
Received in revised form
15 February 2013
Accepted 21 February 2013
Available online 1 March 2013

Keywords:
Ultrasensitive biosensor
Lectin
Electrochemical impedance spectroscopy (EIS)
Self-assembled monolayer (SAM)
Gold nanoparticles
Glycoproteins
Attomolar (aM) concentration
Sialic acid

ABSTRACT

We present here an ultrasensitive electrochemical biosensor based on a lectin biorecognition capable to detect concentrations of glycoproteins down to attomolar (aM) level by investigation of changes in the charge transfer resistance (R_{ct}) using electrochemical impedance spectroscopy (EIS). On polycrystalline gold modified by an aminoalkanethiol linker layer, gold nanoparticles were attached. A *Sambucus nigra* agglutinin was covalently immobilised on a mixed self-assembled monolayer formed on gold nanoparticles and finally, the biosensor surface was blocked by poly(vinyl alcohol). The lectin biosensor was applied for detection of sialic acid containing glycoproteins fetuin and asialofetuin. Building of a biosensing interface was carefully characterised by a broad range of techniques such as electrochemistry, EIS, atomic force microscopy, scanning electron microscopy and surface plasmon resonance with the best performance of the biosensor achieved by application of HS–$(CH_2)_{11}$–NH_2 linker and gold nanoparticles with a diameter of 20 nm. The lectin biosensor responded to an addition of fetuin (8.7% of sialic acid) with sensitivity of $(338 \pm 11)\ \Omega\,\text{decade}^{-1}$ and to asialofetuin ($\leq 0.5\%$ of sialic acid) with sensitivity of $(109 \pm 10)\ \Omega\,\text{decade}^{-1}$ with a blank experiment with oxidised asialofetuin (without recognisable sialic acid) revealing sensitivity of detection of $(79 \pm 13)\ \Omega\,\text{decade}^{-1}$. These results suggest the lectin biosensor responded to changes in the glycan amount in a quantitative way with a successful validation by a lectin microarray. Such a biosensor device has a great potential to be employed in early biomedical diagnostics of diseases such as arthritis or cancer, which are connected to aberrant glycosylation of protein biomarkers in biological fluids.

© 2013 Elsevier B.V. All rights reserved.

1. Introduction

Glycomics is becoming more and more influential member of an "omics" family since glycosylation is the most frequent posttranslational modification of proteins and glycans (saccharides attached to proteins) are actively involved in many physiological and pathological processes [1]. Glycans are better equipped to be an information coding tool compared to DNA and peptides simply because glycans are information rich molecules, i.e. theoretical number of all possible hexamers (consisting of 6 building units) for glycans (1.44×10^{15}) is few orders of magnitude larger compared to peptides (6.4×10^{6}) or DNA (4096) [2]. The size of the cellular glycome is estimated to be in excess of 100,000–500,000 glycan modified biomolecules with a number of unique glycans to be 3000–7000 [3] and this variability can explain human complexity in light of a paradoxically small genome. A pace of advances in the field of glycomics is reduced due to an enormous complexity of glycans on one side with similar physico-chemical properties of glycans on the other side [4], but new high throughput methods have a potential to speed up the process of glycan analysis [5]. The main analytical tools of focus in glycomics include wide range of chromatographic techniques, mass spectrometry, capillary electrophoresis and especially lectin microarray technique.

A microarray technique relying on lectins, which are natural glycan recognising proteins, has a clear advantage over other modern analytical tools applied in glycomics, i.e. glycans do not need to be released from a biomolecule and thus *in-situ* glycan

Abbreviations: AFM, Atomic force microscopy; ASF, Asialofetuin; AuNPs, Gold nanoparticles; DW, Deionised water; EIS, Electrochemical impedance spectroscopy; FET, Fetuin; MH, 6-Mercaptohexanol; MUA, 11-Mercaptoundecanoic acid; OxASF, Oxidised asialofetuin; PVA, Poly(vinyl alcohol); SAM, Self-assembled monolayer; SNA I, *Sambucus nigra* agglutinin; SPR, Surface plasmon resonance

* Corresponding author. Tel.: +421 2 5941 0263; fax: +421 2 5941 0222.
E-mail addresses: Jan.Tkac@savba.sk, jantkac@hotmail.com (J. Tkac).

0039-9140/$ - see front matter © 2013 Elsevier B.V. All rights reserved.
http://dx.doi.org/10.1016/j.talanta.2013.02.052

analysis is possible. Lectin microarrays have been very effective in revealing an active role of glycans in many processes and at present are considered as a standard analytical tool in glycomics [5,6]. However, a typical lectin microarray experiment involves a fluorescent dye being coupled either to lectin or to the glycan/sample for generation of an analytical signal. This requirement for having a label can cause unwanted variability in labelling and biorecognition [6] and thus other formats of analysis working in a label-free mode of detection should be utilised.

Electrochemistry is a very powerful analytical platform with an array of different detection principles and some of them allow to work without any label in a label-free mode of operation [7,8]. Electrochemical impedance spectroscopy (EIS) is quite frequently applied in construction of label-free biosensors due to very sensitive analysis and a simpler set-up compared to field-effect sensing [7]. EIS is based on an electric perturbation of a thin layer on the conductive surface by a small alternating current amplitude and can provide interfacial characteristics such as impedance, resistance and capacitance utilisable in sensing by employment of an equivalent circuit for data evaluation [9]. EIS results are typically transformed into a Nyquist plot, which can provide information about charge transfer resistance R_{ct} in a direct way. After a biorecognition event, R_{ct} increases due to presence of additional layer and thus a subtle change in R_{ct} can be used for detection [10]. Subsequently, EIS allows complex biorecognition events to be probed in a simple, sensitive and label-free manner and EIS is being increasingly popular for development of electrochemical lectin-based biosensors for glycan determination.

EIS is very often combined with formation of self-assembled monolayers (SAMs) allowing to precisely tune interfacial properties such as capacitance and resistance of the interface and/or to control density of ligands at nanoscale subsequently applied in an immobilisation process [11]. Moreover, once SAM is formed it can be employed as a linker to deposit gold nanoparticles on the surface to enhance loading of biorecognition elements and their accessibility, as well [12]. Gold nanoparticles (AuNPs) are of a great attention both from a fundamental [13] and an application-driven perspective [14]. More specifically, AuNPs due to large surface area, intense visible light scattering/absorption, large electron density and catalytic properties have been employed as cargos able to penetrate cell membrane [15], efficient catalysts [16], image contrast agents [17] and most extensively as parts in biosensors or in bioanalytical devices [18] with electrochemical detection platform as the most dominant one [19].

Electrochemical detection of various analytes provides a highly sensitive tool in comparison with other detection platforms in the area of biosensing with detection limits down to attomolar level (aM) for DNA [20], proteins [21], or even low-molecular weight analytes such as pesticides [22]. In this study, we focused on development of a highly sensitive biosensor device by immobilisation of a lectin SNA I recognising 2,6-linked sialic acid on an AuNP layer with integration of such an interface with a label-free format of assays based on EIS. Sialic acids have a prominent role in many pathological processes such as chronic inflammation, HIV, influenza infection, malaria and cancer [1,23] and thus *in-situ* detection of sialic acid on biomolecules is of special interest in glycomics. This is the first paper showing detection limit for glycoprotein determination down to 1 aM level and when we used the same calculations as in a previous paper [24], we were able to detect 40 yoctomoles (i.e. 1.10^{-18} mol $l^{-1} \times 40.10^{-6}$ l) of a glycoprotein, i.e. lower amount than previously claimed for a protein (200 yoctomoles) [24]. Although the biosensor was designed to detect sialic acid in this study, the same immobilisation protocol can be applied for immobilisation of any other lectin, what is an essential feature for integration of this patterning protocol into an array/biochip format of analysis.

2. Materials and methods

2.1. Chemicals

11-Mercaptoundecanoic acid (MUA), 6-mercaptohexanol (MH), potassium hexacyanoferrate(III), potassium hexacyanoferrate(II) trihydrate, potassium chloride, *N*-hydroxysuccinimide (NHS), *N*-(3-dimethylaminopropyl)-*N*′-ethylcarbodiimide hydrochloride (EDC), poly(vinyl alcohol) (PVA, Mowiol® 4-88), sodium periodate, ethylene glycol, cysteamine, acetonitrile, fetuin (FET, 8.7% of sialic acid), asialofetuin (ASF, $\leq$0.5% of sialic acid), cysteamine hydrochloride and gold nanoparticles (5 nm, 10 nm and 20 nm) were purchased from Sigma Aldrich (USA). Phosphate buffer saline tablets (PBST) for SPR buffers were from Merck (Slovakia). Aminoalkanethiol linkers 6-aminohexanethiol and 11-aminoundecanethiol hydrochloride were purchased from Dojindo (Germany). SNA I lectin from *Sambucus nigra* was purchased from Gentaur (Belgium). Biotinylated SNA I lectin was purchased from Vector Laboratories (USA), and CF555-streptavidin fluorescent label was purchased from Biotium (USA). Ethanol for UV/VIS spectroscopy (ultra pure) was purchased from Slavus (Slovakia). Zeba™ spin desalting columns (40k MWCO) for protein purification were purchased from Thermo Scientific (UK). All buffer components were dissolved in deionised water (DW).

2.2. Electrode cleaning and SAM formation

Planar polycrystalline gold electrodes with a diameter of 1.6 mm (Bioanalytical systems, USA) were cleaned as previously described [25]. First, a reductive desorption of previously bound thiols was employed with a potentiostat Autolab PGSTAT 128N (Ecochemie, Netherlands) in a cell with Ag/AgCl reference and a counter Pt electrode (both from Bioanalytical systems, USA) by applying a cyclic potential scanning from −1500 mV to −500 mV in 100 mM NaOH under N_2 atmosphere with a sweep rate of 1 V s^{-1} until a stable cyclic voltammogram was obtained. Then a mechanical polishing of electrodes for 10 min on a polishing pad using 1.0 μm and then 0.3 μm particles (Buehler, USA) for a total polishing time of 20 min was performed, followed by two sonications in DW for 3 min. In the last step the electrodes were left in hot piranha (a mixture of concentrated H_2SO_4 and concentrated H_2O_2 in 3+1 ratio, *handle with a special care*) for 20 min and sonicated in DW for 3 min. Just before the electrode patterning by SAM, CV was employed for an electrochemical polishing of the electrodes (from −200 mV to 1500 mV at a scan rate of 100 mV s^{-1} until a stable CV was obtained—up to 25 scans) and for gold oxide stripping (10 cycles starting from +750 mV to +200 mV at a scan rate of 100 mV s^{-1}) from the electrodes in 100 mM H_2SO_4.

Electrochemical polishing procedure run for two cycles was applied for estimation of a surface coverage of gold nanoparticles attached to polycrystalline gold covered by a thiol linker by integration of a gold reductive peak as proposed previously [25]. A value of electrochemical gold electrode surface area with gold nanoparticles attached was subtracted from a value of electrochemical gold electrode surface area without having gold nanoparticles and this value was then recalculated as coverage of AuNPs.

The electrodes were washed by DW and absolute EtOH, left to dry in dustless environment and subsequently immersed in 1 mM solutions of different aminoalkanethiols for 24 h (to provide a high-density monolayer). After incubation, the electrodes were

washed by absolute EtOH and finally by DW. After the aminoalkanethiol linker layer formation, a gold nanoparticle layer was prepared on the first SAM layer by immersing the modified electrodes into a solution of 5 nm, 10 nm or 20 nm nanoparticles (undiluted stock solutions as obtained from a provider) in the inverted position overnight. 6-Aminohexanethiol and 11-aminoundecanethiol were prepared as 1 mM solutions in absolute EtOH, while cysteamine hydrochloride was diluted in DW to get the same concentration.

2.3. Oxidation of the glycan structures

Glycan of ASF was chemically oxidised using sodium periodate according to a standard protocol [26]. Shortly, a 10 μM stock solution of ASF was oxidised by 10 mM sodium periodate in 50% acetonitrile for 2 h in the dark at laboratory temperature. The reaction was stopped by an addition of ethyleneglycol to the final concentration of 15% (v/v) and incubated for an additional 1 h in the dark. Further, free aldehyde groups formed by the glycan oxidation were blocked by addition of 1 mM cysteamine. The mixture was incubated for 1 h in the dark and finally the ASF with glycan oxidised (OxASF) was recovered with a desalting column.

2.4. Preparation of a bioreceptive surface

A mixed 2nd SAM layer was deposited on AuNP modified polycrystalline gold from a mixture 1+1 of 1 mM 11-mercaptoudecanoic acid (MUA) and 1 mM 6-mercaptohexanol (MH, both in ethanolic solutions) by incubation in the dark for 30 min. The surface was washed by absolute EtOH and DW. A covalent coupling of SNA I lectin on polycrystalline gold electrode modified by gold nanoparticles with attached mixed SAM layer was performed via standard amine coupling chemistry with the first step being an activation of a carboxylic group of MUA by a mixture of 200 mM EDC and 50 mM NHS (1+1) for 15 min. The surface was washed by DW and followed by incubation with 40 μl of a 10 μM lectin stock solution in a 50 mM phosphate buffer pH 6.5 for 20 min in an inverted position. In the initial phase the solution was slowly aspirated from the electrode surface without touching the surface and dispensed back slowly to the electrode. The whole procedure was repeated several times within a timeframe of 1 min and the same procedure was applied during glycoprotein incubation, as well. In order to block non-specific interactions with the biosensor, 5% PVA in DW was incubated with the electrode surface for 30 min. The PVA solution was freshly prepared just before the surface blocking by dilution of the PVA in DW having approx. 80 °C, the solution was well mixed and cooled down to laboratory temperature before being applied to the electrode surface. All these steps are schematically shown in Scheme 1.

Glycoproteins were incubated with the biosensor surface in an inverted position for 20 min (35 min for the aM concentration level) from its aqueous solution with concentrations spanning several orders of magnitude (from 1 aM up to nM levels). The electrode surface was washed by DW after incubation with a glycoprotein and the EIS measurement was performed in an electrolyte containing 5 mM potassium hexacyanoferrate(III), 5 mM potassium hexacyanoferrate(II) and 100 mM KCl. The EIS measurement was run at 50 different frequencies (from 0.1 Hz up to 100 kHz) under Nova Software 1.8 (Ecochemie, Netherlands). Data acquired were evaluated using the same software represented in a Nyquist plot with a circuit R(C[RW]) employed for data fitting.

2.5. SPR measurements

For the SPR measurements, a gold chip (12 mm × 12 mm × 0.3 mm, Litcon, Sweden) was used. The chip was modified with $HS–(CH_2)_{11}–NH_2$ and subsequently with 20 nm AuNPs outside SPR machine (see section *Electrode cleaning and SAM formation*) and subsequently inserted into SPR machine (SR7000DC, Reichert, USA) operated with an autosampler. First, EtOH was injected for a few minutes, followed by injection of 1 mM solution of alkanethiols (1+1 MUA and MH) for 30 min, and washed with EtOH again. After this procedure was completed, the surface was washed by a PBST solution (11.3 mM NaH_2PO_4, 9 mM KOH, 137 mM NaCl containing 0.05% (v/v) Tween-20, pH 7.4) and this solution was applied as a running buffer in the subsequent modification steps. Carboxylic groups were activated by injection of a mixture (1+1) of 0.2 M EDC and 0.05 M NHS for 15 min. After washing the chip with a running buffer, a 10 μM stock solution of SNA I lectin in PBS (11.3 mM NaH_2PO_4, 9 mM KOH, 137 mM NaCl, pH 7.4) was injected with an immobilisation process taking 20 min, and finally the surface was washed by PBST. The flow rate of 5 μl min^{-1} for every incubation step was applied. In the reference flow cell the chip has been modified by the same procedure, but did not involve lectin immobilisation. The sensorgram was recorded and evaluated using SPR Autolink software 1.1.7 (Reichert, USA). For calculation of the total amount of bound lectin the conversion 1 μRIU=1 pg mm^{-2} (according to the manufacturer) was applied.

2.6. Lectin microarray assays

Lectin microarray experiments were run with PBS as a printing buffer, PBST as a washing buffer and PBST containing 1 M ethanolamine applied as a blocking buffer. Shortly, five different concentrations of three different glycoproteins (FET, ASF and oxASF) were spotted using SpotBot3 Microarray Protein edition (Arrayit, USA) on an epoxide coated slides Nexterion E (Schott, Germany) using a previously optimised protocol. Spotting temperature was set to 10 °C and humidity to 50–60%. Subsequently, the slide was placed in the humidity chamber for 1 h at the room temperature with humidity of 80–90%, blocked using a blocking buffer at room temperature for 1 h and with slow shaking, rinsed under a gentle stream of a printing buffer in a Petri dish, and drained to remove excess of a buffer. Then, 70 μl of 67 nM biotinylated SNA I lectin in a binding buffer was applied to the slide surface and incubated for 1 h. After the lectin incubation, the slide was incubated with the Biotium CF555-streptavidin solution (5 μg ml^{-1} in a printing buffer) for 15 min. After the washing procedure was completed, the slide was scanned using InnoScan710 scanner (Innopsys, France) at the wavelength of 532 nm. The slide image was evaluated using the Mapix 5.5.0 software and slide image was evaluated in Photo-PAINT X5 software (Corel, USA) by evaluation of the intensity of green spots (144 pixels) with a black colour having a value of 0 and a green one having a value of 255. Intensity of four independent array spots was evaluated for every glycoprotein analysed.

2.7. Atomic force microscopy (AFM)

Ambient contact and non-contact mode atomic force microscopy imaging was carried out with a Veeco microscope (Di CP-II, Plainview, USA) in conjunction with the integrated Veeco DiProScan control software at a scan rate of 1 line s^{-1} with the tip set to 120 nN. Square shaped gold chips (12 × 12 mm with a thickness of 0.3 mm, Litcon AB, Sweden) modified as previously described for gold electrodes were imaged with an AFM tip MPP-11123 having a diameter of 10 nm and images were finally processed by the IP AutoProbeImage 2.1.15 software.

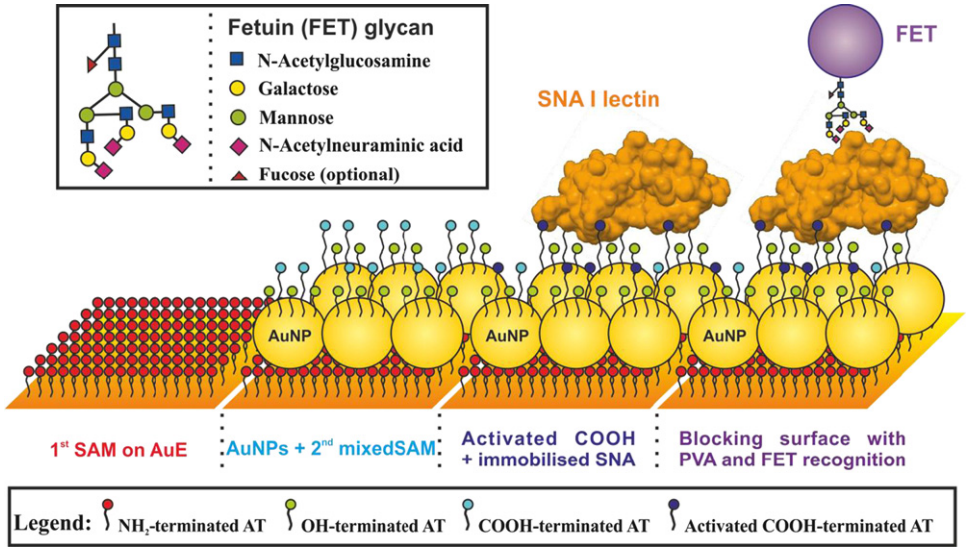

Scheme 1. A graphical representation of all steps applied during biosensor construction and application (from left to right): formation of a linker layer (NH_2-terminated alkanethiol-AT) on a gold surface (1st SAM on AuE); deposition of gold nanoparticles (AuNPs) and formation of a 2nd mixed SAM layer consisting of 11-mercaptoundecanoic acid and 6-mercaptohexanol on AuNPs; activation of carboxyl group and subsequent covalent attachment of SNA I lectin and finally an application of the lectin biosensor in the biorecognition of a glycoprotein fetuin (FET).

2.8. Scanning electron microscopy (SEM)

Structural observations of a surface modified by 20 nm gold nanoparticles were performed by a field emission scanning electron microscopy (SEM–JEOL 7600 FEG) at different magnifications. The acceleration voltage of 15 kV and current of 0.09 nA were used to acquire SEM images.

3. Results and discussion

3.1. Electrochemical characterisation of a 2-D array of AuNPs

Three different aminoalkanethiols (HS–$(CH_2)_2$–NH_2, HS–$(CH_2)_6$–NH_2 and HS–$(CH_2)_{11}$–NH_2) and one dithiol (HS–$(CH_2)_8$–SH) were deposited on a polycrystalline gold surface as a linker layer for subsequent AuNPs adsorption. EIS was applied to get a basic characteristic of the interface—charge transfer resistance R_{ct}, which was consistently higher for a aminoalkanethiol layer, when comparing to the R_{ct} of an aminoalkanethiol layer with deposited AuNPs (Fig. 1). Although this behaviour might be surprising, it is in a good agreement with observations done by Gooding [12]. When HS–$(CH_2)_8$–SH dithiol was applied for formation of a linker layer with 20 nm AuNPs deposited, extremely high R_{ct} of (169 ± 30) kΩ was observed, a value larger by two orders of magnitude, when compared to values observed for any of aminoalkanethiol linker layers formed. Moreover, this dithiol layer exhibited incomplete semicircle in a Nyquist plot, what caused problems for subsequent reliable signal reading. The 2nd parameter being characterised was the size of AuNPs deposited on HS–$(CH_2)_{11}$–NH_2 linker layer. The R_{ct} of a linker SAM layer dropped after deposition of all different AuNPs approximately to the same value (Fig. S1). These results suggest interfacial properties of a hybrid interface were more influenced by a changed length of a linker thiol compared to the changed size of AuNPs deposited. Thus, it can be anticipated, thickness of a linker layer might influence performance of the final biosensor device to a higher degree, when comparing to the influence of the size of AuNPs deposited.

Electrochemical reduction of a gold oxide formed during CV in H_2SO_4 can provide quantitative information about electrochemical gold surface area. A typical surface area of a polycrystalline gold electrode was (0.025 ± 0.003) cm^2 with a roughness factor of 1.2 ± 0.1. The electrochemical gold surface area with AuNPs deposited was as follows: (0.054 ± 0.003) cm^2 for 5 nm AuNPs, (0.039 ± 0.001) cm^2 for 10 nm AuNPs and (0.034 ± 0.001) cm^2 for 20 nm AuNPs. When the electrochemical gold surface area with AuNPs adsorbed was subtracted from the electrochemical surface area of a polycrystalline gold, the electrochemical gold surface area attributed only to AuNPs can be calculated and subsequently a surface coverage was estimated as follows: (2.5 ± 0.1) pmol cm^{-2} for 5 nm AuNPs, (0.29 ± 0.01) pmol cm^{-2} for 10 nm AuNPs and (0.048 ± 0.001) pmol cm^{-2} for 20 nm AuNPs (Fig. S2). SEM revealed a homogeneous formation of 2-D array of 20 nm nanoparticles on the entire surface (Fig. 2).

SEM images at higher magnifications were utilised in calculation of a surface coverage with a value of (0.073 ± 0.006) pmol cm^{-2} for 20 nm AuNPs found. This suggests electrochemical investigation of surface coverage for AuNPs gave reliable results

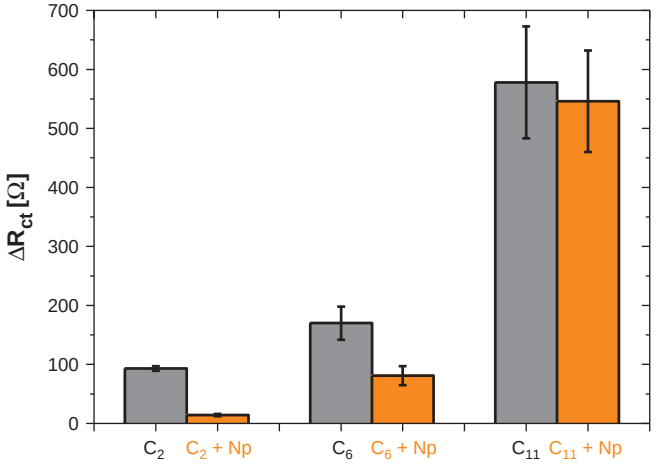

Fig. 1. The influence of a thiol length on ΔR_{ct} (R_{ct} of the gold electrode modified by thiols or by thiols with nanoparticles is subtracted from R_{ct} of a bare gold electrode) of a 2-D array of AuNPs using 20 nm nanoparticles. Abbreviations: C_2=HS–$(CH_2)_2$–NH_2, C_6=HS–$(CH_2)_6$–NH_2, C_{11}=HS–$(CH_2)_{11}$–NH_2 and Np=nanoparticle. Experiments were done at least in triplicate.

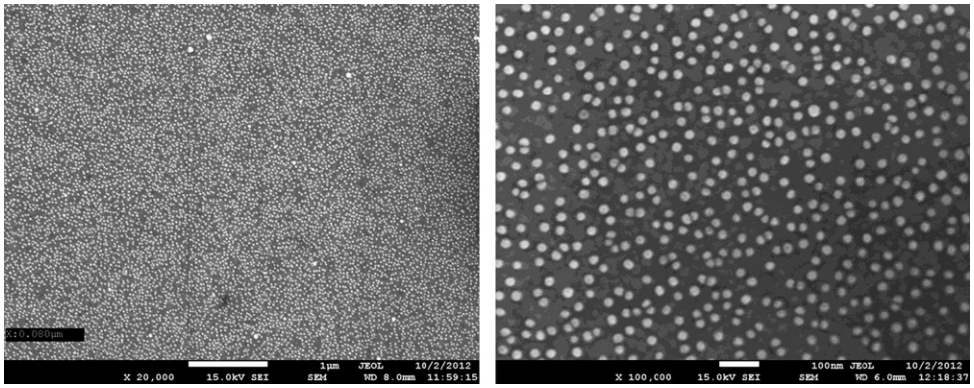

Fig. 2. SEM images of 20 nm AuNPs on the modified surface at magnification of 20,000 × (on left) and 100,000 × (on right). The gold chip surface was firstly modified by HS–$(CH_2)_{11}$–NH_2 and only then AuNPs were deposited to form a 2-D array.

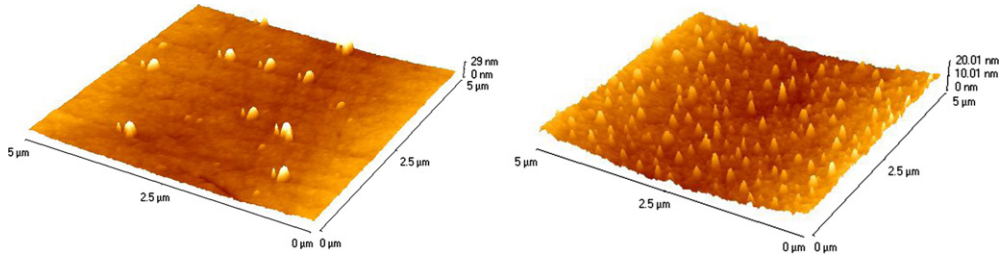

Fig. 3. An AFM image acquired in a non-contact mode on gold chip surface firstly modified by HS–$(CH_2)_{11}$–NH_2 linker and then by deposition of 5 nm AuNPs (on left) and the same gold chip surface investigated in a contact mode (on right) is shown, as well.

even without a need for an expensive instrumentation such as SEM. A lower surface coverage revealed by electrochemistry compared to SEM investigation might be due to partial desorption of HS–$(CH_2)_{11}$–NH_2 linker together with AuNPs during CV sweeps or due to differences in the topology of the gold surface investigated by electrochemistry (a polycrystalline gold electrode with a long history of polishing steps) or by SEM (a planar gold chip). When a hard sphere model was applied for calculation of a theoretical coverage of a full monolayer of AuNPs [27], 5 nm AuNPs formed (33 ± 2)%, 10 nm AuNPs formed (16 ± 1)% and 20 nm AuNPs formed (10.1 ± 0.3)% of a theoretical coverage for a full monolayer of AuNPs.

3.2. AFM characterisation of a 2-D array of AuNPs

It was quite difficult to get AFM image of a 2-D array of AuNPs in a contact mode of operation and only AFM image on a gold surface modified by 5 nm AuNPs was acquired. In order to see presence of AuNPs on gold surfaces, a non-contact mode of operation for AFM gave satisfactory results. A root mean square surface roughness R_q increased with an increasing size of AuNPs in order R_q=2.6 nm for 5 nm AuNPs, R_q=4.1 nm for 10 nm AuNPs and R_q=4.4 nm for 20 nm AuNPs (data for 5 nm AuNPs are shown in Fig. 3). For comparison, a root mean square surface roughness R_q for a planar gold chip was 0.9 nm (data not shown). A striking difference in surface pattern is obvious by comparing AFM image acquired on gold surface patterned by 5 nm AuNPs in a contact and a non-contact mode. While in a contact mode a high density of isolated features can be seen, in a non-contact mode only few features were seen. These images might suggest formation of a first dense layer of AuNPs directly on a linker layer seen in a contact mode AFM with formation of a weakly adsorbed second layer of AuNPs seen only in a non-contact mode AFM. Fortunately, we can assume incubation of these surfaces with a 2nd mixed SAM layer might induce detachment of a weakly adsorbed 2nd layer of AuNPs leaving a homogeneous array of AuNPs.

3.3. Quantification of the amount of immobilised lectin

In order to quantify the amount of lectin immobilised on the surface patterned by a 2-D array of 20 nm AuNPs, SPR experiment able to provide such information has been carried out [28,29]. The experiment shown in Fig. S3 revealed successful formation of a mixed 2nd SAM layer (phase 1), subsequent activation of a –COOH group by a mixture of EDC/NHS (phase 2) and finally immobilisation of SNA I lectin (phase 3). SPR method allowed to quantify the amount of SNA I immobilised as 1.9 pmol cm^{-2}. This value is in a good agreement with a surface coverage of 2.1–2.5 pmol cm^{-2} for immobilised protein on a highly diluted carboxyl containing SAM layer with isolated protein islands seen in AFM [29]. This surface coverage of SNA I should allow unrestricted interaction of the lectin with its analyte, a feature important for high sensitivity of detection. Moreover, quantification of the amount of lectin immobilised allowed us to calculate an approximate number of (40 ± 1) lectin molecules per a nanoparticle within a 2-D array deposited from 20 nm AuNPs.

3.4. Preparation of the biosensor

Even though electrochemical investigation of 2-D AuNPs array suggested higher influence of a thickness of a thiol linker compared to the size of AuNPs on the biosensor performance, we wanted to confirm this by comparison of basic characteristics of the full biosensor. From Table 1 it can be really seen a linker length has a substantial effect on the performance of the biosensor affecting all parameters examined. A very low detection limit for the lectin biosensor of 1 aM was observed, when a 2-D AuNP array was deposited on a HS–$(CH_2)_{11}$–NH_2 linker layer. The same detection limit was achieved by the biosensor device prepared

Table 1
The influence of the thiol linker on the biosensor performance using 20 nm AuNPs.

Linker i.e. 1st SAM	Linear range	RSD FET [%]	RSD ASF [%]	DL [aM]	S [Ω decade^{-1}]	Comment
HS–C_2–NH_2	7	6.5	4.8	≈ 100	13.2 ± 0.6	Small change in absolute R_{ct}
HS–C_6–NH_2	9	8.6	7.2	≈ 10	4.7 ± 0.2	Small change in absolute R_{ct}
HS–C_8–HS	8	13	9.5	≈ 1	49 000 ± 3000	Very high initial R_{ct} and R_{ct} during assay*
HS–C_{11}–NH_2	7	14	7.6	≈ 1	338 ± 11	Moderate initial R_{ct} and R_{ct} during assay

RSD—relative standard deviation of detection of a particular analyte on different electrodes—i.e. it shows reproducibility of construction of independent biosensor devices, DL—detection limit, S—sensitivity of the biosensor i.e. a slope in a linear range of the biosensor.

* Problems with signal reading due to presence of an incomplete semicircle.

Table 2
The influence of the size of AuNPs on the biosensor performance using a HS–$(CH_2)_{11}$–NH_2 linker.

D_{AuNP} [nm]	Linear range	RSD FET [%]	RSD ASF [%]	DL [aM]	Comment
5	?	53	15	≈ 1	Non-linear response
10	?	13	10	≈ 1	Non-linear response
20	7	14	6.9	≈ 1	Linear response

RSD—relative standard deviation of detection of a particular analyte on different electrodes—i.e. it shows reproducibility of construction of independent biosensor devices, DL—detection limit.

with a HS–$(CH_2)_8$–SH linker layer, but signal reading by this biosensor was quite difficult due to presence of an incomplete semicircle in a Nyquist plot. Small change in absolute R_{ct} of the biosensor seen with linkers HS–$(CH_2)_2$–NH_2 and HS–$(CH_2)_6$–NH_2 can have a negative on the performance of the biosensor due to lower reliability of signal reading. Thus, a linker layer formed by deposition of HS–$(CH_2)_{11}$–NH_2 was chosen for further experiments.

Table 2 proves the size of AuNPs has influence on the performance of the biosensor, affecting mainly linearity of the output biosensor signal and reproducibility of assays, when 5 nm AuNPs were used for generation of 2-D array of AuNPs. Utilisation of 5 nm and 10 nm AuNPs is not a good choice for preparation of the lectin biosensor since such device did not respond to its analyte in a linear fashion. The best performance of the lectin biosensor was observed, when a 2-D array of AuNPs was prepared from 20 nm AuNPs showing linear signal in a wide range of concentrations and these nanoparticles were subsequently applied in further studies.

3.5. Validation of the biosensor

It can be concluded the best performance of the biosensor was obtained by the use of a HS–$(CH_2)_{11}$–NH_2 linker and 20 nm AuNPs. A typical response of the biosensor towards two analytes FET and ASF in a low aM concentration range is shown in Fig. 4. In order to prove a response towards these two analytes is specific, a control experiment with oxidised ASF (OxASF) not having recognisable sialic acid was performed and the calibration curve of the biosensor for these three glycoproteins is shown in Fig. 5. The biosensor responded to FET with a sensitivity (i.e. a slope in a linear range of the biosensor) of (338 ± 11) Ω decade^{-1}, to ASF with a sensitivity of (109 ± 10) Ω decade^{-1} and to OxASF with a sensitivity of (79 ± 13) Ω decade^{-1}. When a non-specific signal sensitivity provided by incubation with OxASF was subtracted from the biosensor sensitivity to FET, a specific response of the biosensor for this analyte was (259 ± 17) Ω decade^{-1}. In the same way a specific sensitivity of the biosensor for ASF was calculated to be (30 ± 16) Ω decade^{-1}. Thus, we can conclude the

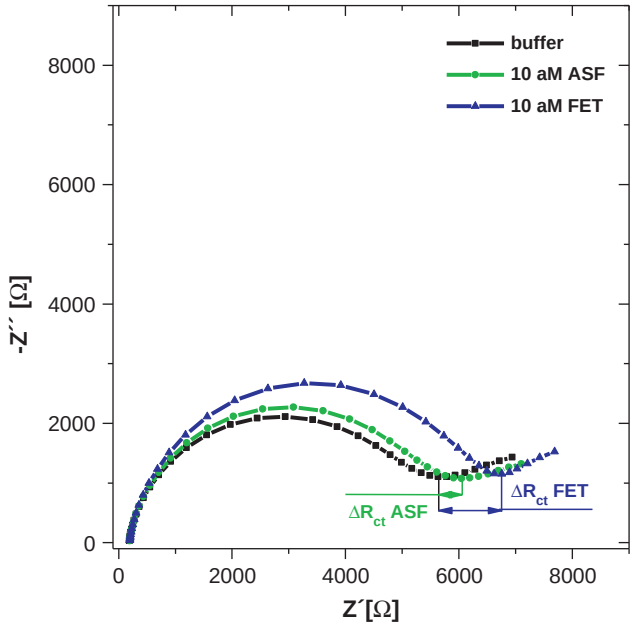

Fig. 4. A response of the biosensor represented in a Nyquist plot based on 2-D array of nanoparticles prepared on a gold electrode surface modified by a HS–$(CH_2)_{11}$–NH_2 linker and 20 nm AuNPs in the presence of a plain buffer and in the presence of two analytes fetuin (FET) and asialofetuin (ASF), both with concentration of 10 aM.

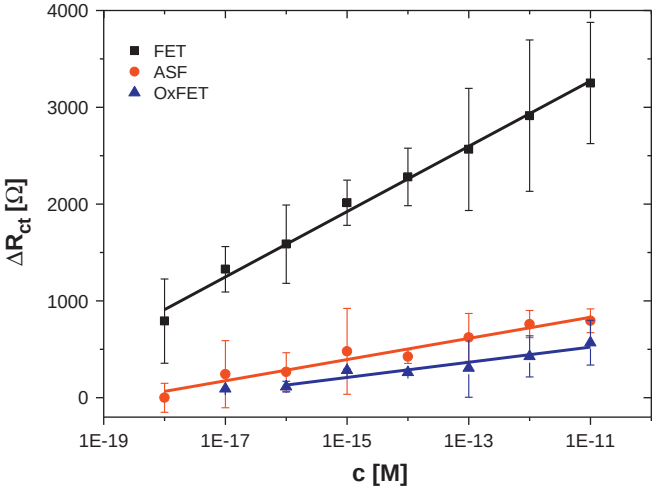

Fig. 5. A calibration plot of the lectin biosensor prepared on a gold electrode modified by HS–$(CH_2)_{11}$–NH_2 linker and 20 nm AuNPs in the presence of two analytes fetuin (FET) and asialofetuin (ASF); and in the presence of oxidised asialofetuin (OxASF). The experiment was performed at least on three different electrodes.

biosensor not only detects its analytes down to aM level, but is able to provide information about the amount of glycan determinants present on a particular glycoprotein. When S/N=3 ratio

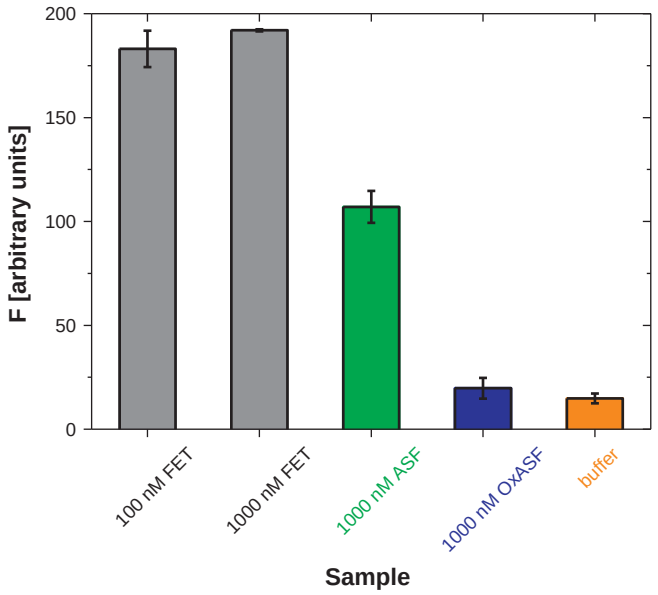

Fig. 6. Quantification of the lectin microarray response towards different analytes such as fetuin (FET) at two different concentrations 100 nM and 1000 nM, 1000 nM asialofetuin (ASF), 1000 nM oxidised asialofetuin (OxASF) and a buffer. Data presented in this figure were read from the image shown in Fig. S4.

was taken into account, a detection limit of the biosensor towards FET was (0.5 ± 0.1) aM and towards ASF of (0.8 ± 0.3) aM.

The biosensor performance to detect three glycoproteins with different level of sialic acid present was validated by a lectin array, which is a current state-of-the-art tool for profiling of glycans on glycoproteins (Fig. S4). Quantification of the intensity of spots confirmed the highest response towards 1000 nM FET, followed by 100 nM FET, 1000 nM ASF and 1000 nM OxASF (Fig. 6). The response towards 1000 nM OxASF was (19.7 ± 5.0) intensity units, a value comparable to the background signal of (14.8 ± 2.4) intensity units obtained with a printing buffer. A very similar binding profile was obtained by the lectin biosensor device. It is worth noting, lectin array offers quite narrow linear range of detection, a common feature of fluorophore-based devices. Typical detection limits obtained so far for analysis of glycans by lectin array are in the range pM–nM [6,30]. Thus, the presented lectin biosensor was successfully validated offering detection limit 10^6–10^9 times lower compared to lectin microarrays, while offering a label-free mode of operation.

3.6. Comparison to other glycan/glycoprotein detecting tools

Glycoproteins can be detected with instrumental tools such as HPLC and capillary electrophoresis coupled with mass spectrometry or using a battery of bioanalytical tools based on integration of lectins for a glycoprotein biorecognition. Combination of capillary electrophoresis with mass spectrometry offered detection limit of 1.8 mM [31]. Liquid chromatography combined with tandem mass spectrometry provided detection limit for serum glycoproteins down to 200 pM level offering linear range within three orders of magnitude, but a quite complex and time-consuming sample pre-treatment was needed [32].

Integration of lectins with analytical instrumentation has attractive features such as short time of analysis and a simple sample pre-treatment [33]. Typical detection limits for SPR are down to nM level [34], for SPR imaging (an array format of analysis) down to 20 nM [35], for enzyme-linked lectin assays down to low nM or sub nM level [36], for QCM down to μM or nM level [37] and for reflectometric interference spectroscopy down to 100 nM level [38].

Electrochemical detection platform in combination with immobilised lectins offered lower detection limits when compared to other detection platforms mentioned above. Two glycoproteins labelled with quantum dots were electrochemically detected with a detection limit down to 34 nM or 3 pM [39] and a biosensor integrated with concanavalin A labelled with daunomycin detected glycoprotein down to 100 pM [40] with utilisable concentration range spanning 2–3 orders of magnitude. EIS-based electrochemical detection platform offered detection limit down to 20 fM [41] or 150 fM for two glycoproteins using two immobilised lectins [42] or down to low nM range for ovalbumin with a concanavalin A integrated biosensor [43]. In our recent study we constructed a lectin biosensor integrated with EIS detection scheme offering a detection limit down to 0.3 fM for a glycoprotein [44]. Thus, the biosensor device presented here offered the lowest detection limit for any lectin-based bioanalytical device or any analytical instrumentation for analysis of glycoproteins published so far. Moreover, the constructed biosensor device offered 4–9 orders of magnitude lower detection limit compared to other EIS-based devices integrated with lectins.

The constructed biosensor can analyse a sample within 30–40 min with 20–30 min needed for sample incubation, about 5 min for EIS measurements and a couple of minutes necessary for the electrode washing and the electrode integration within a measurement set-up. An overall analysis time of the proposed biosensor is considerably shorter compared to ELISA-like lectin assays with a response time of at least 4 h [41].

The proposed lectin biosensor device exhibit features, which are detrimental for analysis of disease biomarkers, which can be present in physiological fluids at extremely low concentrations, what is quite a challenge for biomedical/clinical diagnosis.

4. Conclusions

An extensive optimisation of an interfacial layer of the biosensor prepared by layer-by-layer approach resulted in an ultrasensitive and robust biosensor device able to detect glycoproteins. Fetuin and asialofetuin were chosen as model glycoproteins, since these proteins contain sialic acid, a glycan determinant employed in numerous physiological and pathological processes. The biosensor responded to its analytes linearly spanning seven orders of concentration magnitude, a feature important for analysis of real samples with proteins present at significantly different concentrations. A detection limit of the biosensor starting from ≈ 1 aM level (e.g. 24 glycoprotein molecules in 40 μ of a sample or 40 yoctomoles) can guarantee the device will detect even low-abundant proteins, which can be present at extremely low levels in samples at initial stages of a particular disease. Additional attractive feature of the biosensor is ability to detect changed amount of sialic acid on glycoproteins in a quantitative way. This work lays a solid foundation for future successful utilisation of lectin biosensor devices for the diagnosis of diseases associated with aberrant glycosylation of protein biomarkers such as chronic inflammatory rheumatoid arthritis, genetic disorders and cancer.

Acknowledgement

The financial support from the Slovak scientific grant agency VEGA 2/0127/10 and from the Slovak research and development agency APVV 0282-11 is acknowledged. This contribution/publication was the result of the project implementation: Centre for materials, layers and systems for applications and chemical

processes under extreme conditions—stage II, supported by the Research and Development Operational Program funded by the ERDF.

The research leading to these results has received funding from the European Research Council under the European Union's Seventh Framework Programme (FP/2007-2013)/ ERC Grant Agreement n. 311532.

Appendix A. Supporting information

Supplementary data associated with this article can be found in the online version at http://dx.doi.org/10.1016/j.talanta.2013.02.052.

References

[1] D. Kolarich, B. Lepenies, P.H. Seeberger, Curr. Opin. Chem. Biol. 8 (2011) 1–7.
[2] H.-J. Gabius, H.-C. Siebert, S. André, J. Jiménez-Barbero, H. Rüdiger, ChemBioChem 5 (2004) 740–764;
H.-J. Gabius, S. André, J. Jiménez-Barbero, A. Romero, D. Solís, Trends Biochem. Sci. 36 (2011) 298–313.
[3] R.D. Cummings, Mol. BioSyst. 5 (2009) 1087–1104;
S. Cunningham, J.Q. Gerlach, M. Kane, L. Joshi, Analyst 135 (2010) 2471–2480.
[4] C.R. Bertozzi, L.L. Kiessling, Science 291 (2001) 2357–2364.
[5] C.D. Rillahan, J.C. Paulson, Annu. Rev. Biochem. 80 (2011) 797–823;
J.F. Rakus, L.K. Mahal, L.K. Annu, Rev. Anal. Chem. 4 (2011) 367–392.
[6] P. Gemeiner, D. Mislovicova, J. Tkac, J. Svitel, V. Patoprsty, E. Hrabarova, et al., Biotechnol. Adv. 27 (2009) 1–15;
J. Katrlik, J. Svitel, P. Gemeiner, T. Kozar, J. Tkac, Med. Res. Rev. 30 (2010) 394–418.
[7] J. Tkac, J.J. Davis, in: J.J. Davis (Ed.), Engineering the Bioelectronic Interface: Applications to Analyte Biosensing and Protein Detection, Royal Society of Chemistry, Cambridge, 2009, pp. 193–224;
P. Estrela, D. Paul, Q. Song, L.K.J. Stadler, L. Wang, E. Huq, et al., Anal. Chem. 82 (2010) 3531–3536;
H. Vedala, Y. Chen, S. Cecioni, A. Imberty, S. Vidal, A. Star, Nano Lett. 11 (2011) 170–175.
[8] C. Batchelor-McAuley, E.J.F. Dickinson, N.V. Rees, K.E. Toghill, R.G. Compton, Anal. Chem. 84 (2012) 669–684;
D.W. Kimmel, G. LeBlanc, M.E. Meschievitz, D.E. Cliffel, Anal. Chem. 84 (2012) 685–707.
[9] E. Katz, I. Willner, Electroanalysis 15 (2003) 913–947;
B. Pejcic B, R. De Marco R, Electrochim. Acta 51 (2006) 6217–6229;
J.S. Daniels, N. Pourmand, Electroanalysis 19 (2007) 1239–1257;
F. Lisdat, D. Schäfer, Anal. Bioanal. Chem. 391 (2008) 1555–1567.
[10] T. Bertók, J. Katrlík, P. Gemeiner, J. Tkac, Microchim. Acta 180 (2013) 1–13.
[11] P. Fenter, A. Eberhardt, P. Eisemberger, Science 266 (1994) 1216–1218;
G.M. Whitesides, B. Grzybowski, Science 295 (2002) 2418–2421;
J.C. Love, L.A. Estroff, J.K. Kriebel, R.G. Nuzzo, G.M. Whitesides, Chem. Rev. 105 (2005) 1103–1169;
J.J. Gooding, N. Darwish, Chem. Rec. 12 (2012) 92–105.
[12] J. Dyne, Y.-S. Lin, L.M.H. Lai, J.Z. Ginges, E. Luais, J.R. Peterson, et al., ChemPhysChem 11 (2010) 2807–2813;
S. Techane, D.R. Baer, D.G. Castner, Anal. Chem. 83 (2011) 6704–6712.
[13] A.P. Alivisatos, Science 271 (1996) 933–937;
P.D. Jadzinsky, G. Calero, C.J. Ackerson, D.A. Bushnell, R.D. Kornberg, Science 318 (2007) 430–433;
R. Sardar, A.M. Funston, P. Mulvaney, R.W. Murray, Langmuir 25 (2009) 13840–13851.
[14] Y. Xiao, F. Patolsky, E. Katz, J.F. Hainfeld, I. Willner, Science 299 (2003) 1877–1881;
M.-C. Daniel, D. Astruc, Chem. Rev. 104 (2004) 293–346.
[15] A. Verma, O. Uzun, Y. Hu, Y. Hu, H.-S. Han, N. Watson, et al., Nat. Mater. 7 (2008) 588–595.
[16] J.A. Lopez-Sanchez, N. Dimitratos, C. Hammond, G.L. Brett, L. Kesavan, et al., Nat. Chem. 3 (2011) 551–556;
M. Stratakis, H. Garcia, Chem. Rev. 112 (2012) 4469–4506.
[17] A.M. Alkilany, S.E. Lohse, C.J. Murphy, Acc. Chem. Res. (2013), http://dx.doi.org/10.1021/ar300015b.
[18] R. Elghanian, J.J. Storhoff, R.C. Mucic, R.L. Letsinger, C.A. Mirkin, Science 277 (1997) 1078–1081;
Y.W.C. Cao, R. Jin, C.A. Mirkin, Science 297 (2002) 1536–1540;
S.-J. Park, T.A. Taton, C.A. Mirkin, Science 295 (2002) 1503–1506;
E. Katz, I. Willner, Angew. Chem. Int. Ed. 43 (2004) 6042–6108;
K. Kerman, M. Saito, S. Yamamura, Y. Takamura, E. Tamiya, Trends Anal. Chem. 27 (2008) 585–592;
A. Sassolas, B.D. Leca-Bouvier, L.J. Blum, Chem. Rev. 108 (2008) 109–139;
M.E. Stewart, C.R. Anderton, L.B. Thompson, J. Maria, S.K. Gray, et al., Chem. Rev. 108 (2008) 494–521;
S. Krishnendu, S.S. Agasti, C. Kim, X. Li, V.M. Rotello, Chem. Rev. 112 (2012) 2739–2779.
[19] S. Campuzano, J. Wang, Electroanalysis 23 (2011) 1289–1300;
S. Guo, E. Wang, Nano Today 6 (2011) 240–264;
I. Willner, B. Willner, R. Tel-Vered, Electroanalysis 23 (2011) 13–28.
[20] L. Soleymani, Z. Fang, E.H. Sargent, S.O. Kelley, Nat. Nanotech. Lett. 4 (2009) 844–848;
W. Gao, H. Dong, J. Lei, H. Ji, H. Ju, Chem. Commun. 47 (2011) 5220–5222;
H. Dong, Z. Zhu, H. Ju, F. Yan, Biosens. Bioelectron. 33 (2012) 228–232.
[21] M. Dijksma, B. Kamp, J.C. Hoogvliet, W.P. van Bennekom, Anal. Chem. 73 (2001) 901–907;
F. Yu, B. Persson, S. Lofas, W.J. Knoll, J. Am. Chem. Soc. 126 (2004) 8902–8903;
S.P. Mulvaney, K.M. Myers, P.E. Sheehan, L.J. Whitman, Biosens. Bioelectron. 24 (2009) 1109–1115.
[22] S. Sotiropoulou, D. Fournier, N.A. Chaniotakis, Biosens. Bioelectron. 20 (2005) 2347–2352.
[23] N.M. Varki, E. Strobert, E.J. Dick Jr, K. Benirschke, A. Varki, Annu. Rev. Pathol. Mech. Dis. 6 (2011) 365–393;
K. Mariño, J. Bones, J.J. Kattla, P.M. Rudd, Nat. Chem. Biol. 6 (2010) 713–723.
[24] H. Zhang, X.-F. Li, X.C. Le, Anal. Chem. 84 (2012) 877–884.
[25] J. Tkac, J.J. Davis, J. Electroanal. Chem. 621 (2008) 117–120.
[26] Y. Li, Y. Tian, T. Rezai, A. Prakash, M.F. Lopez, D.W. Chan, H. Zhang, Anal. Chem. 83 (2010) 240–245.
[27] J. Lahiri, L. Isaacs, J. Tien, G.M. Whitesides, Anal. Chem. 71 (1999) 777–790.
[28] J.J. Davis, J. Tkac, S. Laurenson, P.Ko Ferrigno, Anal. Chem. 79 (2007) 1089–1096.
[29] J.J. Davis, J. Tkac, R. Humphreys, A.T. Buxton, T.A. Lee, P.Ko Ferrigno, Anal. Chem. 81 (2009) 3314–3320.
[30] K.T. Pilobello, L. Krishnamoorthy, D. Slawek, L.K. Mahal, ChemBioChem 6 (2005) 985–989;
A. Kuno, N. Uchiyama, S. Koseki-Kuno, Y. Ebe, S. Takashima, et al., Nat. Methods 2 (2005) 851–856;
K. Fromell, M. Andersson, K. Elihn, K.D. Caldwell, Colloids Surf., B 46 (2005) 84–91.
[31] K. Imami, Y. Ishihama, S.J. Terabe, J. Chromatogr. A 1194 (2008) 237–242.
[32] L.A. Hammad, D.Z. Derryberry, Y.R. Jmeian, Y. Mechref, Rapid Commun. Mass Spectrom. 24 (2010) 1565–1574.
[33] G. Safina, Anal. Chim. Acta 712 (2012) 9–29.
[34] G. Safina, I.B. Duran, M. Alasel, B. Danielsson, Talanta 84 (2011) 1284–1290.
[35] W. Liu, Y. Chen, M. Yan, Analyst 133 (2008) 1268–1273.
[36] D. Mislovičová, J. Katrlík, E. Paulovičová, P. Gemeiner, J. Tkac, Colloids Surf., B 94 (2012) 163–169.
[37] M.M. Pedroso, A.M. Watanabe, M.C. Roque-Barreira, P.R. Bueno, R.C. Faria, Microchem. J. 89 (2008) 153–158.
[38] H.W. Choi, H. Takahashi, T. Ooya, T. Takeuchi, Anal. Methods 3 (2011) 1366–1370.
[39] C. Yang, C. Xu, X. Wang, X. Hu, Analyst 137 (2012) 1205–1209.
[40] K. Sugawara, A. Yugami, T. Kadoya, K. Hosaka, Talanta 85 (2011) 425–429.
[41] V.J. Nagaraj, S. Aithal, S. Eaton, M. Bothara, P. Wiktor, S. Prasad, Nanomedicine 5 (2010) 369–378.
[42] J.T. La Belle, J.Q. Gerlach, S. Svarovsky, L. Joshi, Anal. Chem. 79 (2007) 6959–6964.
[43] M.D.L. Oliveira, M.T.S. Correia, L.C.B.B. Coelho, F.B. Diniz, Colloids Surf., B 66 (2008) 13–19.
[44] T. Bertok, P. Gemeiner, M. Mikula, P. Gemeiner, J. Tkac, Microchim. Acta 180 (2013) 151–159.